

NONLINEAR RESPONSE OF PARAMETRICALLY-EXCITED MEMS

Jeffrey F. Rhoads*

Dept. of Mechanical Engineering
Michigan State University
East Lansing, Michigan, 48824
Email: rhoadsje@msu.edu

Steven W. Shaw

Dept. of Mechanical Engineering
Michigan State University
East Lansing, Michigan, 48824
Email: shawsw@egr.msu.edu

Kimberly L. Turner

Dept. of Mechanical and
Environmental Engineering
University of California, Santa Barbara
Santa Barbara, California, 93106
Email: turner@engineering.ucsb.edu

Jeff Moehlis

Dept. of Mechanical and
Environmental Engineering
University of California, Santa Barbara
Santa Barbara, California, 93106
Email: moehlis@engineering.ucsb.edu

Barry E. DeMartini

Dept. of Mechanical and
Environmental Engineering
University of California, Santa Barbara
Santa Barbara, California, 93106
Email: baredog@umail.ucsb.edu

Wenhua Zhang[†]

Dept. of Mechanical and
Environmental Engineering
University of California, Santa Barbara
Santa Barbara, California, 93106
Email: whzh@engr.ucsb.edu

ABSTRACT

Due to the position-dependent nature of electrostatic forces, many microelectromechanical (MEM) oscillators inherently feature parametric excitation. This work considers the nonlinear response of one such oscillator, which is electrostatically actuated via non-interdigitated comb drives. Unlike other parametrically-excited systems, which feature only linear parametric excitation in their equation of motion, the oscillator in question here exhibits parametric excitation in both its linear and nonlinear terms. This complication proves to significantly enrich the system's dynamics. Amongst the interesting consequences is the fact that the system's nonlinear response proves to be qualitatively dependent on the system's excitation amplitude. This paper includes an introduction to the equation of motion of interest, a brief, yet systematic, analysis of the equation's nonlinear response, and experimental evidence of the predicted behavior as measured from an actual MEM oscillator.

INTRODUCTION

The emergence of practical uses for electrostatically-actuated microelectromechanical (MEM) oscillators coupled with the inherent existence of parametric excitation (due to the position-dependent nature of electrostatic forces) in many such devices, has led the authors, amongst others, to consider both the modeling and response of systems involving generalized forms of parametric excitation and its associated resonances [1–7]. In this paper the response of a simple model of a representative parametrically-excited MEM oscillator is considered. Unlike most parametrically-excited systems, which feature only linear parametric excitation, the system of interest features parametric excitation in both the linear and nonlinear terms of its equation of motion. This simple, yet fundamental, difference proves to have a dramatic effect on the system's dynamics [1, 8]. In particular, it can be shown that such systems fail to feature a single effective nonlinearity which characterizes the nonlinear behavior of the system. Rather, such systems exhibit branch-specific nonlinearities which, when collectively analyzed, yield the system characteristics. One result of this complication is that

*Please address all correspondence to this author.

[†]Currently at Hewlett-Packard Research Labs, Palo Alto, CA

such systems can exhibit not only typical softening or hardening behavior, but also mixed behavior which corresponds to the nontrivial response branches bending toward or away from one another near resonance [1, 8]. In addition, it can be shown that the qualitative nature of their nonlinear frequency response depends on the amplitude of excitation.

This paper begins with a brief introduction to the equation of motion of interest and a summary of the analytical procedure used to reach the results summarized in this work. The relevant nonlinear behavior is discussed in the context of the motivating example, a parametrically-excited MEM oscillator, and experimental evidence of the predicted behavior is presented. The paper then concludes with some closing remarks and an outline of ongoing and future work. It should be noted that, where relevant, issues pertaining to the practical design of MEM oscillators are included. The full details of this work can be found in [8].

THE EQUATION OF MOTION AND PERTURBATION ANALYSIS

As mentioned above, the equation of motion examined in this work was originally formulated by the authors to model a parametrically-excited MEM oscillator. It is worth noting, however, that such equations naturally arise in other problems as well, including the analysis of parametrically-excited columns fabricated from nonlinear elastic materials [9, 10] and Paul trap mass spectrometers [11]. Accordingly, the principal motivation for this study is treated only as an example here.

The equation of motion of interest in this work is of the form

$$z'' + 2\varepsilon\zeta z' + z(1 + \varepsilon v_1 + \varepsilon \lambda_1 \cos \Omega \tau) + \varepsilon z^3 (\gamma_3 + \lambda_3 \cos \Omega \tau) = 0, \quad (1)$$

where ε represents a 'small' scaling parameter introduced solely for the sake of analysis and prime designates the derivative with respect to τ [1, 5, 7, 8].

In order to simplify the analysis of Eq. (1), it is convenient to employ standard perturbation techniques, in this case, the method of averaging. To assist with this approach, a standard coordinate transformation is first introduced which transforms the equation into amplitude and phase coordinates:

$$z(\tau) = a(\tau) \cos\left(\frac{\Omega\tau}{2} + \psi(\tau)\right), \quad (2)$$

$$z'(\tau) = -a(\tau) \frac{\Omega}{2} \sin\left(\frac{\Omega\tau}{2} + \psi(\tau)\right). \quad (3)$$

In addition, since near resonant behavior is of primary interest, a detuning parameter σ is introduced, which is defined with respect to the principal parametric resonance condition, namely,

$$\Omega = 2 + \varepsilon\sigma. \quad (4)$$

Separating and averaging the resulting system of equations over the period $4\pi/\Omega$ in the τ - domain yields the system's averaged equations, which are of the form [1, 7, 8],

$$a' = \frac{1}{8}a\varepsilon[-8\zeta + (2\lambda_1 + a^2\lambda_3) \sin 2\psi] + O(\varepsilon^2), \quad (5)$$

$$\psi' = \frac{1}{8}\varepsilon[3a^2\gamma_3 + 4v_1 - 4\sigma + 2(\lambda_1 + a^2\lambda_3) \cos 2\psi] + O(\varepsilon^2). \quad (6)$$

As evident from these averaged equations, the parametric excitation in the cubic term, namely the presence of λ_3 , significantly complicates the system as compared to a typical Mathieu system, which features only linear parametric excitation. The net effect of this complication is highly noticeable in the system's response, as revealed in the following section.

STEADY-STATE SOLUTIONS OF THE SYSTEM

Since the qualitative nature of the system's response is of primary interest in this work, zero damping ($\zeta = 0$) is assumed to simplify the analysis. With this assumption in place, the steady-state behavior of the averaged equations presented in Eqs. (5) - (6) can be considered in analytical form.

Setting $a' = \psi' = 0$ in Eqs. (5) - (6) and solving the resulting equations, which govern steady-state motion, reveals that the system has a trivial solution and four pair of distinct nontrivial steady-state response branches [8]. The first two pair, in terms of amplitude and phase, are given by

$$a_1 = \pm \sqrt{\frac{4\sigma + 2\lambda_1 - 4v_1}{3\gamma_3 - 2\lambda_3}}, \quad (7)$$

$$\psi_1 = \frac{\pi}{2}, \quad (8)$$

and

$$a_2 = \pm \sqrt{\frac{4\sigma - 2\lambda_1 - 4v_1}{3\gamma_3 + 2\lambda_3}}, \quad (9)$$

$$\psi_2 = 0. \quad (10)$$

Clearly, the sign of the argument of the square root will determine the range of detuning over which these solutions are real valued and thus physically apparent. More meaningful in the context of this work, however, is the nature of their nonlinear response, which in this case differs for each of the response branches. In particular, since the denominator of each of these branches differs, the nonlinear behavior of each branch is independent from the other. To examine the net effect of this discrepancy, branch specific nonlinearities are defined using the denominator of each of the amplitude expressions presented above, namely,

$$\eta_1 = 3\gamma_3 - 2\lambda_3 \quad (11)$$

and

$$\eta_2 = 3\gamma_3 + 2\lambda_3. \quad (12)$$

By using these effective nonlinearities it is easily shown that when both $\eta_1 > 0$ and $\eta_2 > 0$ the typical hardening nonlinear behavior locally exists. Similarly, for $\eta_1 < 0$ and $\eta_2 < 0$ the usual softening nonlinear behavior locally exists. However, due to the independent nature of each branch's nonlinearity, two mixed or hybrid cases also exist, namely, $\eta_1 > 0$ and $\eta_2 < 0$, and $\eta_1 < 0$ and $\eta_2 > 0$, which correspond to the two nontrivial response branches dictated above bending toward or away from one another near the principal parametric resonance condition, as determined by λ_1 and ν_1 . A summary of this result is presented in Fig. 1, which shows each of the various response regions present in the $\gamma_3 - \lambda_3$ parameter space. Note that transitions between response regions occur when either one or both effective nonlinearities equal zero, which corresponds to a perfectly vertical solution branch as produced by the singularity in the response [8].

The third and fourth pairs of nontrivial response branches appear at identical constant amplitude in the absence of damping, given by

$$a_{3,4} = \pm \sqrt{\frac{-2\lambda_1}{\lambda_3}}, \quad (13)$$

and are distinguished by their phases, given by

$$\psi_{3,4} = \pm \frac{1}{2} \arccos \left(\frac{-3\gamma_3\lambda_1 + 2\lambda_3\nu_1 - 2\lambda_3\sigma}{\lambda_1\lambda_3} \right). \quad (14)$$

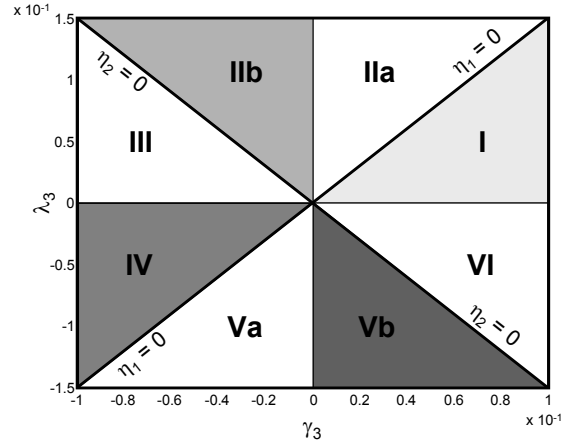


Figure 1. The γ_3 - λ_3 parameter space (From [8]). The various response regions are designated by Roman numerals.

Due to the presence of the square root in the amplitude term, these solutions clearly can appear in only the upper or lower half-plane of the parameter space presented in Fig. 1, as dictated by the sign of λ_1/λ_3 . As brief analysis shows however, these solutions do not abruptly appear across the $\lambda_3 = 0$ axis, but rather a 'smooth' bifurcation occurs here and the additional constant amplitude solutions are created from $\pm\infty$ [8].

With each of the nontrivial solution branches characterized, all that remains for analysis of the system's frequency response is a complete stability analysis. Though omitted here for the sake of brevity, such an analysis is easily completed through examination of the local linear behavior of the system about its various equilibria [8]. In fact, in the absence of damping, each equilibrium's stability can be shown to be solely dependent on the sign of the determinant of the Jacobian matrix of the local linear system evaluated at the specific equilibrium point [8].

A BRIEF LOOK AT THE SYSTEM'S FREQUENCY RESPONSE

With both the steady-state solutions and their associated stabilities known, it is worthwhile to consider a representative example. As such, consider an undamped system whose dynamics are accurately captured by Eq. (1) with $\nu_1 = \lambda_1 = 1$ (Note that these results are easily extended for other parameter values as well). The frequency response plots for this special case are easily generated, using the results of the previous section, for each of the response regions depicted in Fig. 1 as shown in Figs. 2-5. Note that though Regions I, IIa, Vb, and VI are omitted here, the responses in these regions are symmetric counterparts to those which lie in the other half-plane. A brief

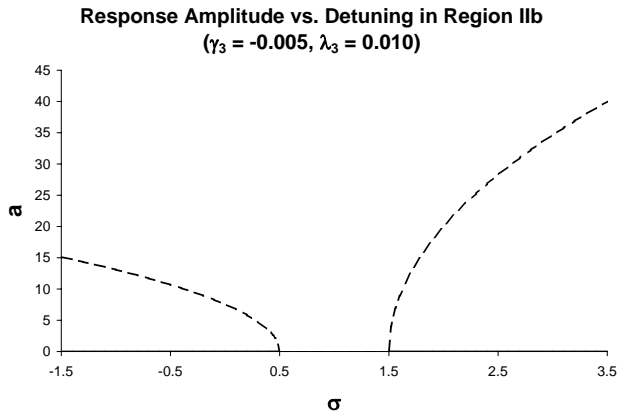


Figure 2. Representative frequency response plot for Region IIb in Fig. 1 [8]. Here and elsewhere, solid lines indicate a stable response and dashed lines an unstable response.

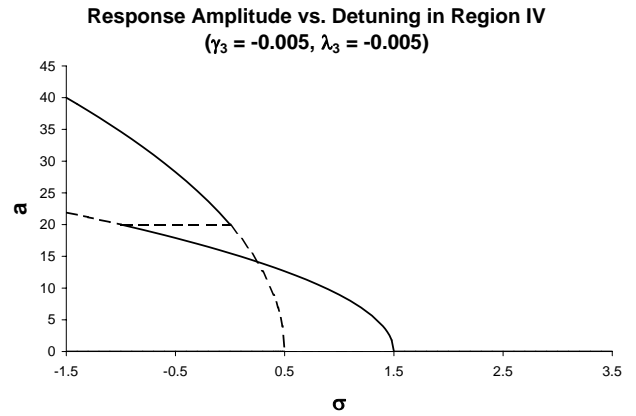


Figure 4. Representative frequency response plot for Region IV in Fig. 1 [8].

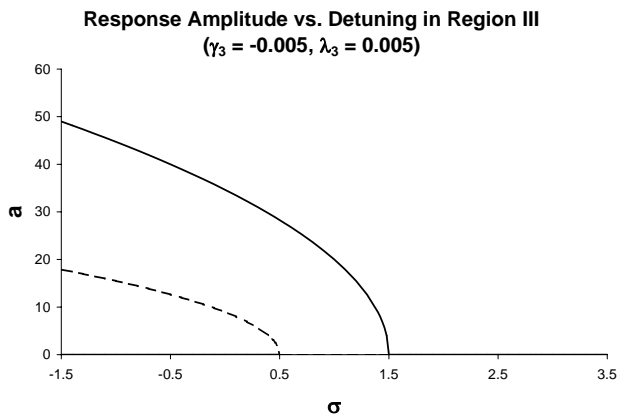


Figure 3. Representative frequency response plot for Region III in Fig. 1 [8].

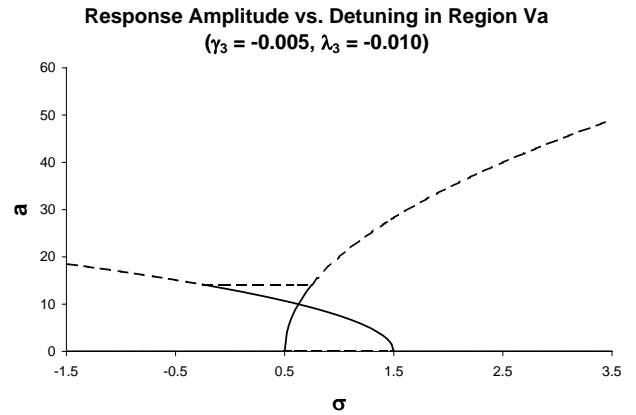


Figure 5. Representative frequency response plot for Region Va in Fig. 1 [8].

explanation of the included plots follows.

To begin, consider the frequency response shown in Fig. 2, which corresponds to Region IIb in Fig. 1. This region exemplifies a system with mixed nonlinearities in that the nontrivial response branches do not bend in the same direction. Rather, after branching off in subcritical pitchfork bifurcations, the nontrivial response branches bend away from one another near resonance, which in turn leads to globally unbounded solutions (taken loosely here to indicate that some solutions grow unbounded within this detuning region). The response depicted in Figure 3, corresponding to Region III in Fig. 1, is much more mundane. Here the two nontrivial responses branch off in two pitchfork bifurcations, one subcritical and one supercritical, yielding behavior entirely consistent with typical

softening behavior and solutions that remain globally bounded.

The dynamics in the lower half-plane are slightly more rich due to the presence of the additional solution branches (a_3 and a_4). Figure 4, corresponding to Region IV in Fig. 1, for example, appears to locally exhibit typical softening behavior. However as the frequency is decreased from zero detuning additional local bifurcations occur corresponding to the creation and annihilation of the additional solutions. In addition, these bifurcations lead to an exchange in the stability of the frequency-dependent branches. Though the net result is still a globally stable response, it is clearly distinct from the response presented in Fig. 3. The response depicted in Fig. 5 is also unique in that the response branches here bend toward one another near resonance. However, these stable branches persist only until their connection with the constant amplitude branches wherein

they destabilize in additional bifurcations, yielding a globally unstable system.

Though only a small number of frequency response plots are included in this very brief analysis, it should be noted that the system contains a considerable amount of interesting phenomena not examined herein, ranging from invariant manifolds in various phase spaces to global bifurcations. As mentioned before, a full accounting of this phenomena can be found in [8]. It should also be noted that though only the undamped system is considered here, the effects of damping on the system can be appreciable (in general, it leads to symmetry breaking) and are also worthy of consideration. These results can also be found in [8].

EXAMPLE: A PARAMETRICALLY-EXCITED MICRO-ELECTROMECHANICAL (MEM) OSCILLATOR

Though the results presented in the preceding sections are applicable to a wide variety of problems involving generalized parametric resonance, the present study, as previously mentioned, was motivated by the analysis of parametrically-excited MEM oscillators, such as the one depicted in Fig. 6. This oscillator consists primarily of a backbone, B, the principal shuttle mass or proof mass of the system, suspended over a substrate by four folded beam springs, S, and excited by a pair of non-interdigitated comb drives, N, which are externally powered by an AC voltage source (not shown). Though two interdigitated comb drives, C, are also present in Fig. 6, it should be noted that they were used only for sensing purposes in the present study and thus are not explicitly discussed here.

While the authors have previously verified that the equation of motion given by Eq. (1) accurately captures the dynamics of oscillators such as that depicted in Fig. 6, the development is repeated here for both the sake of completeness and to provide further justification for the conclusions presented in this work, and perhaps more importantly, to explain their relevance to the design of MEM devices [1, 3, 7, 8].

To begin, it is noted that the equation of motion of the oscillator in question can be generalized to be of the form

$$m\ddot{x} + c\dot{x} + F_r(x) + F_{es}(x, t) = 0, \quad (15)$$

where $F_r(x)$ represents the elastic restoring force produced by the four folded beam springs and $F_{es}(x, t)$ represents the electrostatic driving and restoring forces produced by the non-interdigitated comb drives under a fluctuating voltage excitation, given by [1, 3, 7, 8]

$$V(t) = V_A \sqrt{1 + \cos \omega t}. \quad (16)$$

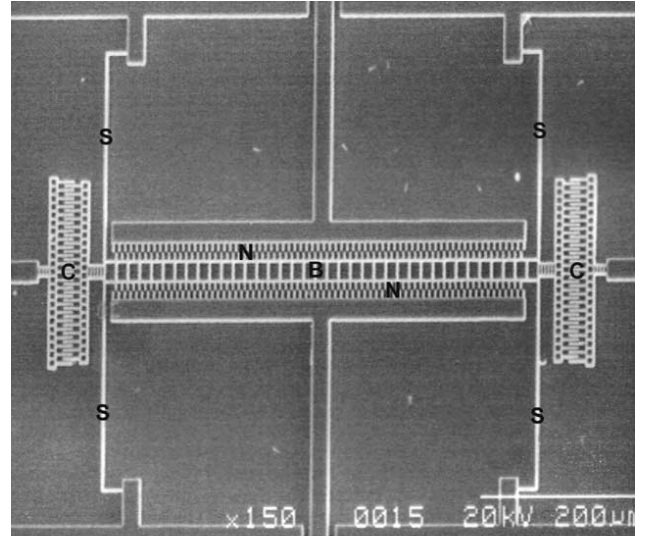


Figure 6. A representative parametrically-excited MEM oscillator (From [3]). The backbone is indicated by the letter B, S indicates the folded beam springs which supply the system's elastic restoring force, N indicates the non-interdigitated comb drives used to provide the electrostatic driving and restoring forces, and C identifies the interdigitated comb drives, which are used here solely for sensing purposes.

As previously shown in [3], each of these forces can be accurately modeled by cubic functions of displacement, in particular,

$$F_r(x) = k_1x + k_3x^3 \quad (17)$$

and

$$F_{es}(x, t) = (r_{1A}x + r_{3A}x^3)V_A^2(1 + \cos \omega t), \quad (18)$$

where k_1 and k_3 , and r_{1A} and r_{3A} , represent mechanical stiffness and electrostatic coefficients respectively. Substitution of these forces into Eq. (15) yields a dimensional equation of motion for the shuttle mass of the form [1, 7, 8]:

$$m\ddot{x} + c\dot{x} + k_1x + k_3x^3 + (r_{1A}x + r_{3A}x^3)V_A^2(1 + \cos \omega t) = 0. \quad (19)$$

To ensure consistent analysis it proves beneficial to rescale Eq. (19) such that it is nondimensional. Accordingly, time and displacement are rescaled according to

$$\tau = \omega_0 t \quad (20)$$

and

$$z = \frac{x}{x_0}, \quad (21)$$

Table 1. Nondimensional Parameter Definitions [8].

Definition	Nondimensional Parameter
$(\bullet)' = \frac{d(\bullet)}{d\tau}$	Scaled Time Derivative
$\varepsilon\zeta = \frac{c}{2m\omega_0}$	Scaled Damping Ratio
$\varepsilon\lambda_1 = \frac{r_{1A}V_A^2}{k_1}$	Linear Electrostatic Excitation Coefficient
$\Omega = \frac{\omega}{\omega_0}$	Nondimensional Excitation Frequency
$\varepsilon\chi = \frac{k_3x_0^2}{k_1}$	Nonlinear Mechanical Stiffness Coefficient
$\varepsilon\lambda_3 = \frac{x_0^2r_{3A}V_A^2}{k_1}$	Nonlinear Electrostatic Excitation Coefficient

where ω_0 represents the linear elastic natural frequency, defined according to

$$\omega_0 = \sqrt{\frac{k_1}{m}}, \quad (22)$$

and x_0 represents a characteristic length of the system. This, assuming the nondimensional damping, net electrostatic force, and nonlinear mechanical force are small, which is valid for the near-resonant operation of MEM oscillators, results in a nondimensional equation of motion for the backbone, very similar to that given in Eq. (1), given by

$$z'' + 2\varepsilon\zeta z' + z(1 + \varepsilon\lambda_1 + \varepsilon\lambda_1 \cos \Omega\tau) + \varepsilon z^3 (\chi + \lambda_3 + \lambda_3 \cos \Omega\tau) = 0, \quad (23)$$

with parameters and operators defined in accordance with Table 2 [1, 7, 8].

Since the equation of motion presented in Eq. (23) is of the form of that presented in Eq. (1), it is readily apparent that the results of the previous sections are directly applicable to the oscillator in question. However, whereas in the previous sections the nonlinear parameters of the system could be independently

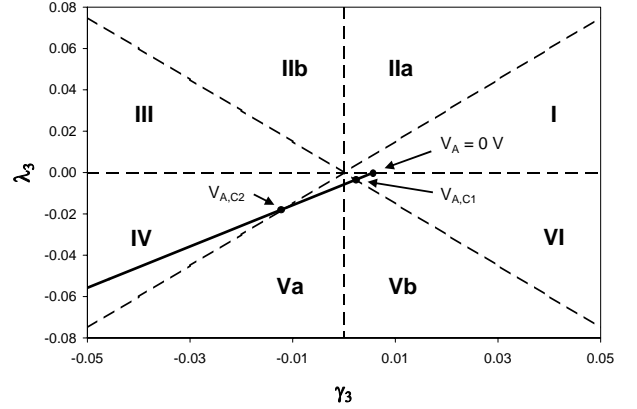


Figure 7. The $\gamma_3 - \lambda_3$ parameter space superimposed with the nonlinearity path the oscillator design presented in Table 2 would exhibit [8].

selected, in the case of the MEM oscillator these parameters are inherently coupled to the system's excitation. In particular, the nonlinear parameters, amongst others, depend on the amplitude of the AC voltage excitation (V_A). The net result of this reliance is that the system actually exhibits qualitative changes in its nonlinear response, that is, it transitions between the response regions delineated in Fig. 1, as V_A is varied [8]. To examine this further, consider the oscillator's nonlinearity in terms of the $\gamma_3 - \lambda_3$ parameter space using

$$\varepsilon\lambda_3 = \frac{x_0^2 r_{3A} V_A^2}{k_1} \quad (24)$$

and

$$\varepsilon\gamma_3 = \varepsilon\chi + \varepsilon\lambda_3 = \varepsilon\chi + \frac{x_0^2 r_{3A} V_A^2}{k_1}. \quad (25)$$

Clearly when $V_A = 0$ the system lies at $(\gamma_3, \lambda_3) = (\chi, 0)$, on the boundary between Regions I and VI, in the parameter space, however, as the voltage is increased the system follows a line in the parameter space specified by

$$\lambda_3 = \gamma_3 - \chi. \quad (26)$$

As a result, depending on the oscillator's parameters and the input voltage of the system, the oscillator can feasibly exhibit a nonlinear response compatible with any of the response regions presented in Fig. 1.

To examine this phenomenon further, consider the oscillator design described by the parameters given in Table 2. As shown in

Table 2. Design Parameters for a Representative MEM Oscillator [8].

Definition	Nondimensional Parameter
r_{1A}	$8 \times 10^{-4} \frac{\mu N}{V^2 \mu m}$
r_{3A}	$-1.2 \times 10^{-4} \frac{\mu N}{V^2 \mu m^3}$
k_1	$7.15 \frac{\mu N}{\mu m}$
k_3	$0.042 \frac{\mu N}{\mu m^3}$
c	$2.11 \times 10^{-8} \frac{kg}{s}$
m	$2.5 \times 10^{-10} kg$

Fig. 7 this oscillator freely transitions between Regions VI, Vb, Va, and IV as the input voltage amplitude, V_A , is varied. Thus, within the 0 - 35 V input voltage window the oscillator exhibits quasi-hardening, quasi-softening, and the so-called mixed nonlinear behavior. Though such qualitative changes may be of interest from a research point of view, in most, but not all, practical applications their existence is somewhat undesirable. As such, it is proves beneficial to identify the transition voltages at which the behavioral transitions are predicted, so that they can be avoided in practical implementation. As brief calculations will reveal, such transitions take place at

$$V_{A,C1} = \sqrt{\frac{-3k_3}{5r_{3A}}} \quad (27)$$

for the VI to Vb transition, and

$$V_{A,C2} = \sqrt{\frac{-3k_3}{r_{3A}}} \quad (28)$$

for the Va to IV transition.

It should be pointed out that despite the fact that these MEM oscillators can transition between response regions, all devices produced to date, due to the nature of their mechanical

nonlinearities ($\chi > 0$), exhibit hardening characteristics at 0 V. Accordingly, any oscillators designed to exhibit softening or quasi-softening nonlinearities have a minimum operating voltage required to achieve the desired behavior. This constraint, however, is of minimal concern as these oscillators, regardless of their operating region, feature, like most parametrically-excited systems, a minimum operating voltage constraint due to the presence of damping.

In an attempt to verify the assertions of this section, experimental results produced using an actual oscillator, based on the design presented in Table 2, are included in Figs. 8-10. These figures show the frequency response curves for the device in question at AC voltage excitation amplitudes of 7.6 V, 16.6 V, and 33.0 V. As predicted by theory, the oscillator's nonlinearity qualitatively changes as the excitation voltage is increased. In particular, at 7.6 V the oscillator exhibits hardening characteristics, at 16.6 V mixed nonlinear characteristics, and at 33.0 V softening characteristics.

While the experimental results presented in Figs. 8-10 are promising indications of the validity of the analysis presented in this work, a few issues remain to be addressed. For example, the absence of effects associated with the additional constant amplitude solution is slightly disconcerting. This, however, is largely reconcilable with the fact that the authors were not aware of such phenomena previous to and during the experimentation shown and thus this phenomena was not taken into account during frequency sweeps and device characterization. Similarly, the parameters shown in Table 2, though highly compatible with the analytical predictions, were derived through a recently developed identification procedure, which though systematic, is not yet refined. Accordingly, direct comparisons between analytical and experimental results are limited by the degree of accuracy of the parameter identification process. Ongoing experimentation and characterization should help address both of these issues.

CONCLUSION

As shown throughout this work, parametrically-excited MEM oscillators and systems with generalized forms of parametric resonance, in general, exhibit an array of interesting dynamical features. Amongst the more interesting is the fact that such system are capable of displaying not only typical hardening or softening nonlinear characteristics, but also mixed nonlinear characteristics wherein the principal response branches bend toward or away from one another near resonance. In fact, in certain incarnations (in particular, parametrically-excited MEM oscillators) such behavior can be shown to be explicitly coupled to the excitation amplitude of the system. That is, such systems can be shown to qualitatively transition between various nonlinear regimes as the excitation amplitude is varied.

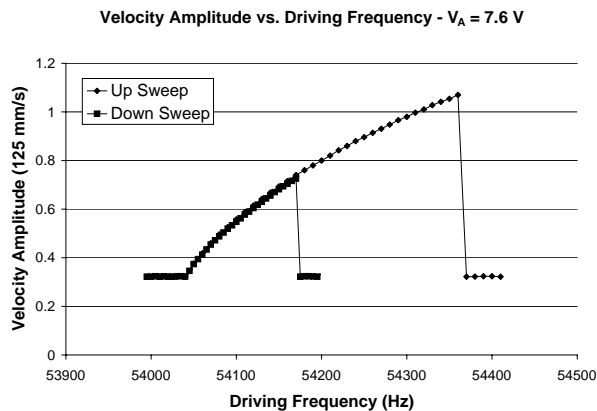


Figure 8. Experimentally-derived frequency response curves for a MEM oscillator excited at 7.6 V (From [8]).

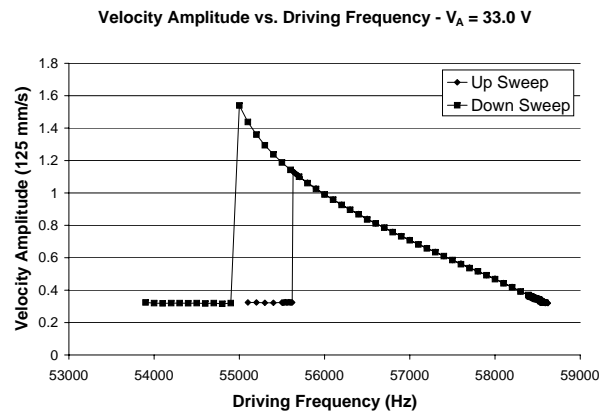


Figure 10. Experimentally-derived frequency response curves for a MEM oscillator excited at 33.0 V (From [8]).

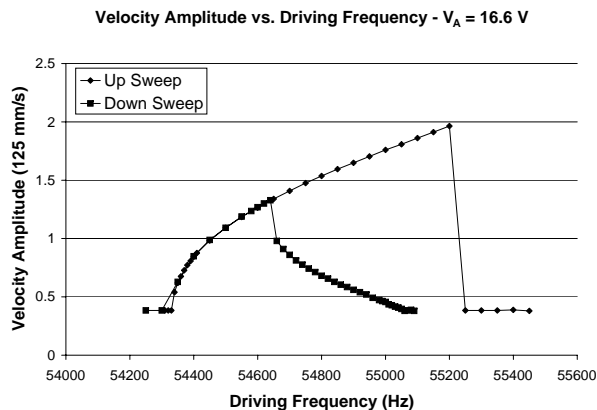


Figure 9. Experimentally-derived frequency response curves for a MEM oscillator excited at 16.6 V (From [8]).

Though previous experimentation has yielded results generally compatible with the results presented in this work, some issues remain, as highlighted in the preceding section. These issues are currently being addressed through a new experimental campaign designed to further characterize such systems in light of the analytical results presented in this work.

ACKNOWLEDGMENT

This work was supported by the Air Force Office of Scientific Research (AFOSR) under contract F49620-02-1-0069 and by the National Science Foundation under grant NSF-0428916. The authors are also grateful for the \TeX technical assistance provided by Mr. Brian Olson.

REFERENCES

- [1] Rhoads, J. F., Shaw, S. W., Turner, K. L., and Baskaran, R., 2004. "Tunable MEMS filters that exploit parametric resonance". *To appear in the ASME Journal of Vibration and Acoustics*.
- [2] Turner, K. L., 1999. "Applications and analysis of parametric resonance in microelectromechanical systems". PhD Thesis, Cornell University.
- [3] Zhang, W., Baskaran, R., and Turner, K. L., 2002. "Effect of cubic nonlinearity on auto-parametrically amplified resonant MEMS mass sensor". *Sensors and Actuators A: Physical*, **102**(1-2), pp. 139–150.
- [4] Turner, K. L., and Zhang, W., 2001. "Design and analysis of a dynamic MEM chemical sensor". In Proceedings of the 2001 American Control Conference, Vol. 1212, pp. 1214–1218.
- [5] Zhang, W., Baskaran, R., and Turner, K. L., 2002. "Nonlinear dynamics analysis of a parametrically resonant MEMS sensor". In Proceedings of the 2002 SEM Annual Conference and Exposition on Experimental and Applied Mechanics.
- [6] Zhang, W., and Turner, K., 2004. "Parametrically resonant mass sensor". In Proceedings of the 2004 Workshop on Solid-State Sensors and Actuators, to be published.
- [7] Shaw, S. W., Turner, K. L., Rhoads, J. F., and Baskaran, R., 2003. "Parametrically excited MEMS-based filters". In Proceedings of the IUTAM Symposium on Chaotic Dynamics and Control of Systems and Processes in Mechanics.
- [8] Rhoads, J. F., Shaw, S. W., Turner, K. L., Moehlis, J., DeMartini, B. E., and Zhang, W., 2005. "Nonlinear parametric resonance in electrostatically-excited microelectromechanical systems". *In preparation for the Journal of Sound and*

Vibration.

- [9] Mond, M., Cederbaum, G., Khan, P. B., and Zarmi, Y., 1993. “Stability analysis of the non-linear Mathieu equation”. *Journal of Sound and Vibration*, **167**(1), pp. 77–89.
- [10] Younesian, D., Esmailzadeh, E., and Sedaghati, R., 2005. “Existence of periodic solutions for the generalized form of Mathieu equation”. *Nonlinear Dynamics*, **39**(4), pp. 335–348.
- [11] Abraham, G. T., and Chatterjee, A., 2003. “Approximate asymptotics for a nonlinear Mathieu equation using harmonic balance based averaging”. *Nonlinear Dynamics*, **31**, pp. 347–365.